Effect of the Exchange of Substituent Position in an Amide Amphiphile on the Monolayer Characteristics

D. Vollhardt*,† and R. Wagner‡

Max Planck Institute of Colloids and Interfaces, D-14424 Potsdam/Golm, Germany, and GE Bayer Silicones Technology, 51368 Leverkusen, Germany

Received: February 23, 2006; In Final Form: May 29, 2006

The monolayer characteristics of two very similar amphiphiles, *N*-tridecyl-β-hydroxypropionic acid amide ($C_{13}H_{27}-NH-CO-C_2H_4OH$; THPA) and N-($\beta$-hydroxyethyl)tridecanoic acid amide ($C_{13}H_{27}-CO-NH-C_2H_4$-OH; HETA), the chemical structure of which is only changed by exchanging the position of the two substituents at the acid amide group, are compared. These small changes in the chemical structure give rise to large differences in the phase behavior of the HETA and THPA monolayers, as concluded from the differences in the surface pressure−area ($\pi-A$) isotherms. Since both amphiphiles have the same alkyl chain length, the shift of the fluid/condensed phase transition pressure π_c to higher temperatures from THPA to HETA indicates a stronger polar character of the THPA headgroup. Considerable differences between the HETA and THPA monolayers also exist in the domain morphology, although, in both cases, six arms usually grow from a round center. The fractal-shaped HETA domains grow by tip splitting under the formation of numerous doubloons so that branching is considerably limited. This suggests a certain fluidity of the HETA condensed phase. The main differences of the domains result from the higher crystallinity. The starlike THPA domains have dendritic character and can form curved dendrites, which are partially two-dimensional twins due to the formation of dislocations in the two-dimensional lattice structure. In the case of HETA monolayers, the grazing incidence X-ray diffraction studies reveal a hexagonal packing of the alkyl chains oriented perpendicularly to the surface in an LS phase. In the case of THPA monolayers, an oblique lattice is formed. However, at low temperatures, a second phase transition between two condensed phases occurs that is demonstrated by an abrupt transition between two different oblique lattice structures at the surface pressure where a cusp in the $\pi-A$ isotherms occurs at $T < 10$ °C.

Introduction

The characteristic features of Langmuir monolayers depend sensitively on the chemical structure of the amphiphiles, and the monolayer state is mainly determined by surface pressure and temperature. The generally accepted principle that the shape of the condensed phase domains is principally controlled by the competition between the dipolar energy of the domain molecules and the line tension energy at the domain boundary reveals the fundamental role of the molecular structure of the amphiphile.[1−4] An enormous morphological variety of condensed phase domains has been found not only in Langmuir monolayers[5,6] but also in adsorbed monolayers (Gibbs monolayers),[7] in Langmuir monolayers penetrated by dissolved surfactants,[8,9] or in Langmuir monolayers after molecular recognition of a non-surface-active species dissolved in the aqueous subphase.[10−12] Already, small changes in the molecular structure of the amphiphile can result in changes in the molecular arrangement in the monolayer and thus in changes of the main characteristics of the monolayer, such as the surface pressure−area per molecule ($\pi-A$) isotherms, the shape and texture of the condensed phase domains, and the two-dimensional (2D) lattice structure. This is demonstrated, for example, by a systematic alteration of the headgroup structure in four monoglycerol amphiphiles by an amide, ether, ester, and amine group,[13] by four phospholipids of the same chain length that are different only with respect to the number of methyl groups at the nitrogen of the headgroup,[14] or by fatty acids with slightly changed OH substitution in the midpositions of the alkyl chain.[15]

The role of amide and amine groups is of special interest because these groups are an integral part of the general structure of sphingolipids.[16,17] Hydrogen-bonded systems of amides seem to play an important role in those membrane parts that allow the transport into the cells.[18] The hydrogen bonding patterns of sphingolipids are well investigated because of their enigmatic properties.[19]

Therefore, in previous papers, we studied the main monolayer characteristics of various tailored amphiphiles containing an amide group. We synthesized tailored amphiphiles, the headgroup of which consists of an acid amide group and one or two hydroxyl groups separated by one or more (two or three) methylene groups.[20−30] Generally, the domain morphology of this type of amphiphile is crystalline, despite notable differences in the domain textures at changes in the chemical structure of the headgroups, even at a phase transition with temperature change.

Studies of a special amphiphile of this type *N*-dodecyl-γ-hydroxybutyric acid amide (DHBAA), which is soluble enough in the aqueous subphase and can also be spread as a Langmuir monolayer, have established that a first-order phase transition can occur in adsorption layers.[20,21,24,26,27] Comprehensive in-

* Corresponding author. Tel: -49-331-567-9258. Fax: -49-331-567-9202. E-mail: vollh@mpikg-golm.mpg.de.
† Max Planck Institute of Colloids and Interfaces.
‡ GE Bayer Silicones Technology.

10.1021/jp061164q CCC: $33.50
Published on Web 07/08/2006

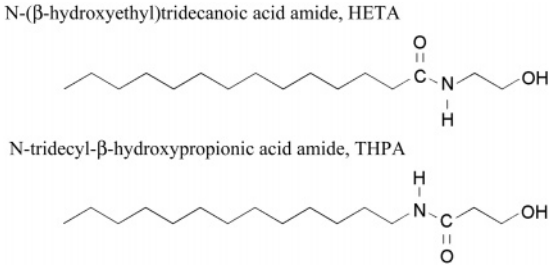

Figure 1. Change in the chemical structure of the above two amphiphiles by exchanging the position of the two substituents at the acid amide group.

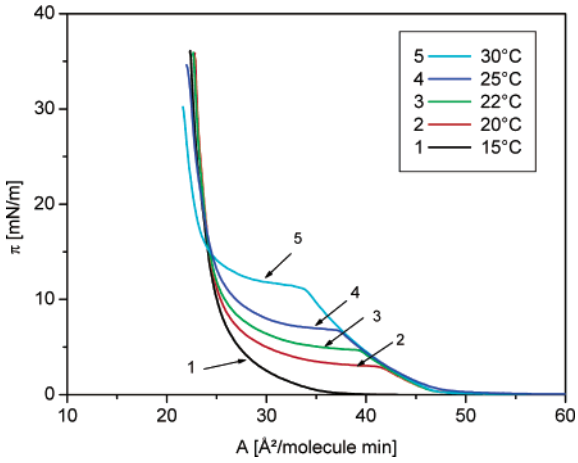

Figure 2. $\pi-A$ isotherms of HETA monolayers spread on water, measured in the temperature range between 15 and 30 °C.

vestigations of the thermodynamic properties, the morphological textures, and the 2D lattice structures of DHBAA adsorption layers have provided conclusive experimental evidence for the formation of condensed phase structures in adsorbed monolayers that have nearly the same features as those formed by the corresponding Langmuir monolayers.

On the other hand, the preparation of the R and S enantiomers of N-tetradecyl-γ,δ-dihydroxypentadecanoic acid amide allowed us to show that chiral discrimination effects are observable in the macroscopic domain morphology, the energetic differences of which are obviously too small to cause noticeable discrimination effects in the thermodynamic properties, or in the 2D lattice structures.[22]

The present study focuses on the effect of a very small change in the chemical structure of an acid amide amphiphile on the characteristic features of the Langmuir monolayers, that is, not based on chirality. The objective of this work is to compare the monolayer characteristics of two amphiphiles, the chemical structure of which is only changed by exchanging the position of the two substituents at the acid amide group. For this purpose, we synthesized the tailored amphiphiles *N*-tridecyl-β-hydroxypropionic acid amide ($C_{13}H_{27}-NH-CO-C_2H_4OH$; THPA) and *N*-($\beta$-hydroxyethyl)tridecanoic acid amide ($C_{13}H_{27}-CO-NH-C_2H_4OH$; HETA). The more detailed chemical structure of the two amphiphiles is presented in Figure 1. The corresponding Langmuir monolayers are characterized by the coupling of surface pressure−area per molecule ($\pi-A$) isotherms, Brewster angle microscopy (BAM) imaging, and grazing incidence X-ray diffraction (GIXD) measurements.

Experimental Section

The two amphiphiles HETA and THPA were synthesized, which are different in the position of the two substituents at the acid amide group.

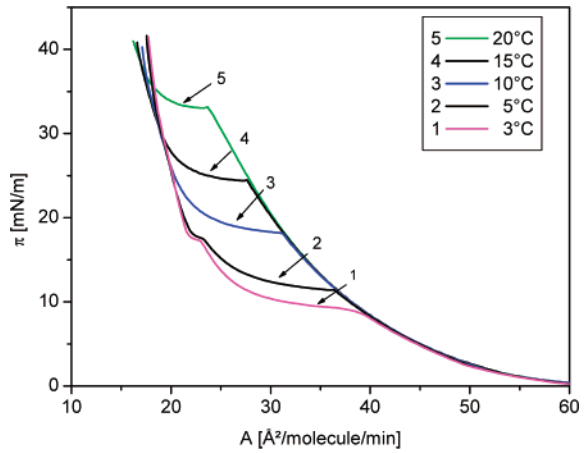

Figure 3. $\pi-A$ isotherms of THPA monolayers spread on water, measured in the temperature range between 3 and 20 °C.

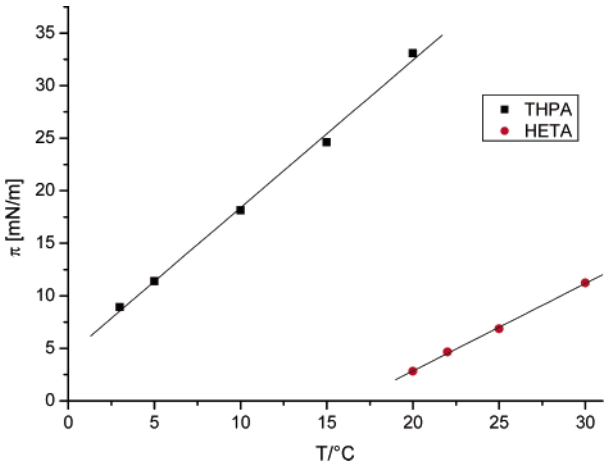

Figure 4. Temperature dependence of the main phase transition pressure π_c of the monolayers of HETA and THPA spread on water.

The synthesis of HETA was performed according to the scheme

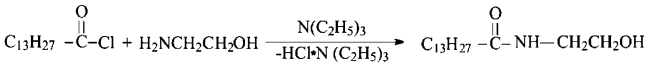

In a first step, 2-aminoethanol (6.1 g, 0.1 mol) and triethylamine (15 g, 0.15 mol) were dissolved in 20 mL of anhydrous 1.4 dioxane. Separately, tetradecanoic acid chloride (24.7 g, 0.1 mol) was dissolved in 70 mL of anhydrous 1.4 dioxane and slowly added to the 2-aminoethanol solution at room temperature. The mixture was heated to 50 °C for 3 h. Volatiles were removed in a vacuum. The solid material was mixed intensively with 200 mL water and filtered, and the solid filtrate washed was with water again. Afterward, the obtained product was recrystallized four times from dioxane/pentane (8:2) and four times from acetone/pentane (8:2) mixtures.

The amphiphile THPA was synthesized according to the scheme

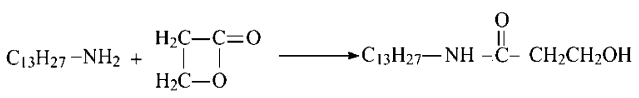

In a first step, tridecylamine (19.9 g, 0.1 mol) was dissolved in 70 mL of anhydrous 1.4 dioxane. Separately, β-propiolactone (7.2 g, 0.1 mol) was dissolved in 20 mL of anhydrous 1.4 dioxane and slowly added to the tridecylamine solution at room

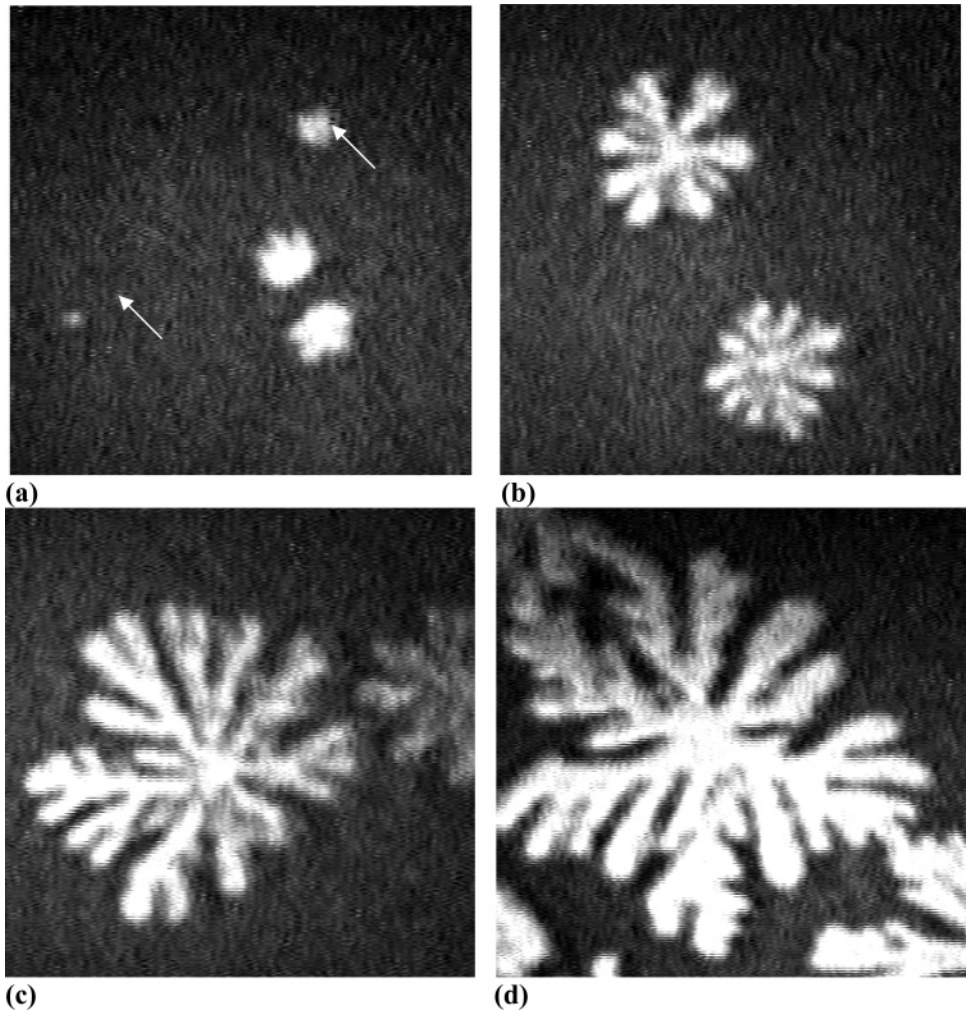

Figure 5. Succeeding steps of the domain growth within the phase coexistence region of the $\pi-A$ isotherms of an HETA monolayer spread on water; $T = 20$ °C.

temperature. The mixture was heated to 80 °C for 5 h. Afterward, volatiles were removed in a vacuum. The obtained THPA was recrystallized four times from dioxane/pentane (8:2) and four times from acetone/pentane (8:2) mixtures.

The chemical purity of both amphiphiles (≥99%) was checked by elemental analysis and high-performance liquid chromatography.

Ultrapure water having a specific resistance of 18.2 MΩ and used for the monolayer experiments was obtained from a Millipore desktop system. The spreading solvent was chloroform (p.a. grade; Baker, Holland).

The measurements of the surface pressure ($\pi-A$) isotherms and the BAM studies were performed in a experimental setup consisting of a self-made computer-interfaced film balance coupled with a Brewster angle microscope (BAM1+, NFT, Göttingen, Germany). The Wilhelmy method was used to measure the surface pressure. Using a roughened glass plate, the accuracy of the surface pressure was reproducible to ±0.1 mNm^{-1}, and the area per molecule was reproducible to $\pm 5 \times 10^{-3}$ nm^2. Equilibrium $\pi-A$ isotherms were recorded at a compression rate of ≤ 0.1 nm^2/(molecule min). The lateral resolution of the BAM1+ is approximately 4 μm. Simple imaging processing software was used to optimize the contrast. More detailed information on the BAM method is given elsewhere (see, e.g., refs 5 and 31 and the references therein).

The GIXD experiments were performed using the liquid-surface diffractometer on the undulator beamline BW1 at HASYLAB, DESY, Hamburg, Germany. A monochromatic synchrotron X-ray beam was adjusted to strike the helium/water interface at a grazing incidence angle of $\alpha_i = 0.85\alpha_c$, where α_c is the critical angle for total reflection. The diffracted intensity was recorded by a linear position-sensitive detector (PSD) (OED-100-M, Braun, Garching, Germany) as a function of the horizontal scattering angle α_f. The detector was rotated around the sample to record the diffracted intensity as a function of the horizontal scattering angle $2\theta_{xy}$. A Soller collimator in front of the PSD restricted the *in-plane* divergence of the diffracted beam to 0.09°. All characteristics of the 2D lattice were calculated from the intensities as a function of the in-plane component and the out-of-plane component of the scattering vector.[32−34] The scattering vector Q has an *in-plane* component $Q_{xy} \approx (4\pi/\lambda) \sin \theta_{xy}$ and an *out-of-plane* component $Q_z \approx (2\pi/\lambda) \sin \alpha_f$, where λ is the X-ray wavelength. The intensities as a function of Q_{xy} and Q_z were least-squares fitted as a Lorentzian in the *in-plane* direction and as a Gaussian in the *out-of-plane* direction. The lattice parameters were obtained from the peak positions. The lattice spacing is given by $d(hk) = 2\pi/Q_{xy}^{hk}$, where (h,k) denotes the order of the reflection. The lattice parameters a, b, c, and γ were calculated from the lattice spacing d_{hk}, and, from these, the unit cell area $A_{xy} = ab \sin \gamma$. The polar tilt angle t of the long molecule axis, and the tilt azimuth ψ_{xy} were calculated from the positions of the Q_{xy} and Q_z maxima,[34] according to $Q_z^{hk} = Q_{xy}^{hk} \cos \psi_{hk} \tan t$.[34] The cross section per

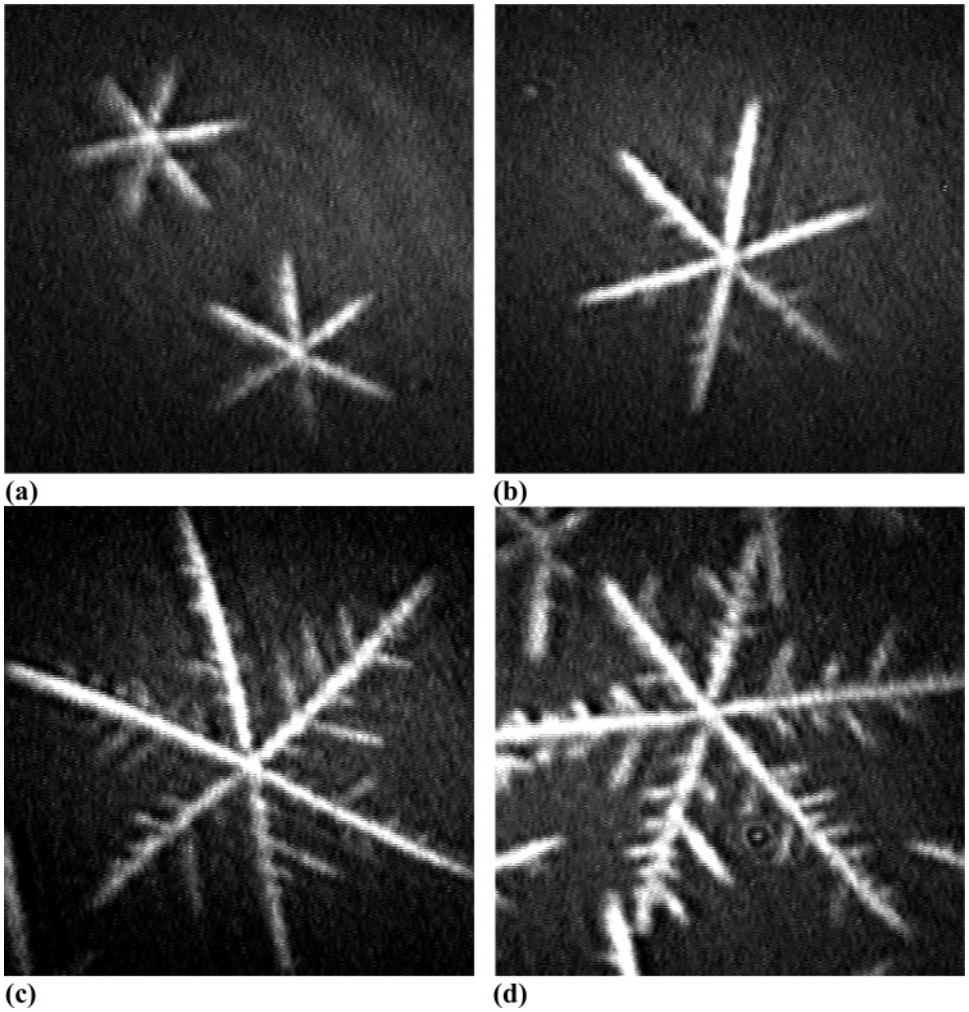

Figure 6. Succeeding stages of the domain development within the phase coexistence region of the $\pi-A$ isotherms of a THPA monolayer spread on water, obtained for low compression rates ($\leq$0.1 nm^2/(min molecule)); $T = 10$ °C.

alkyl chain $A_0 = A_{xy} \cos t$ is related to the unit cell area A_{xy} (area per molecule parallel to the interface) and the tilt angle t. The full width at half-maximum of a Bragg peak Δ_{xy} corrected for resolution effects of the detector can be taken to determine the coherence length $\xi = 2\pi/\sqrt{(\Delta_{xy}^2 - \Delta_{res}^2)}$, where the second term under the root represents the resolution of the Soller collimator.

Results and Discussion

The comparison of the $\pi-A$ isotherms of the HETA and THPA monolayers (Figures 2 and 3) demonstrates that, already, the very small change in the chemical structure of the two amphiphiles by exchanging the position of the two substituents at the acid amide group has a large effect on the thermodynamic monolayer features. At first, we look at the temperature dependence of the experimental $\pi-A$ isotherms of the HETA monolayers spread on pure water. Figure 2 shows five $\pi-A$ isotherms of HETA monolayers in the temperature range between 15 and 30 °C. It is seen that the features of the $\pi-A$ isotherms of HETA correspond to those of most of the usual monolayers of amphiphiles.[35] The isotherms show a sharp inflection at the first-order phase transition point (A_c) from a fluid phase to a condensed phase. The slope of the isotherm in the following two-phase coexistence region ($A < A_c$) is much lower than that compared to the fluid state, and it becomes more horizontal with the decrease in temperature and surface pressure. The extension of the fluid phase increases with the temperature. The A_c values corresponding to the onset of this main phase transition become smaller with the increase in temperature and exist in the accessible surface pressure range first above 17 °C.

The $\pi-A$ isotherms of the THPA monolayers are completely different. Figure 3 shows five $\pi-A$ isotherms of the THPA monolayers in the temperature range between 3 and 20 °C. Even at the lowest temperature, the main phase transition starts already in the positive pressure range. It is of special interest that, at low temperatures, the $\pi-A$ isotherms of THPA monolayers reveal a striking second critical point at $A < A_c$, indicating the existence of a second phase transition between two condensed phases. The large differences in the phase behavior of the HETA and THPA monolayers can be demonstrated by the presentation of the dependence of the main phase transition pressure π_c between the fluid and condensed phase on temperature. This is seen in Figure 4, which shows large differences between the linear π_c-T relationship of the HETA and THPA monolayers fitted by linear regression. It is interesting to refer to the large shift in the linear π_c-T relations to essentially higher temperatures from the THPA to HETA monolayers, since both amphiphiles have the same alkyl chain length. Obviously this shift indicates the stronger polar character of the THPA headgroup.

BAM is a sensitive method to visualize the highly specific differences in the condensed phase domains formed in the main phase transition region of the $\pi-A$ isotherm. So, it is interesting

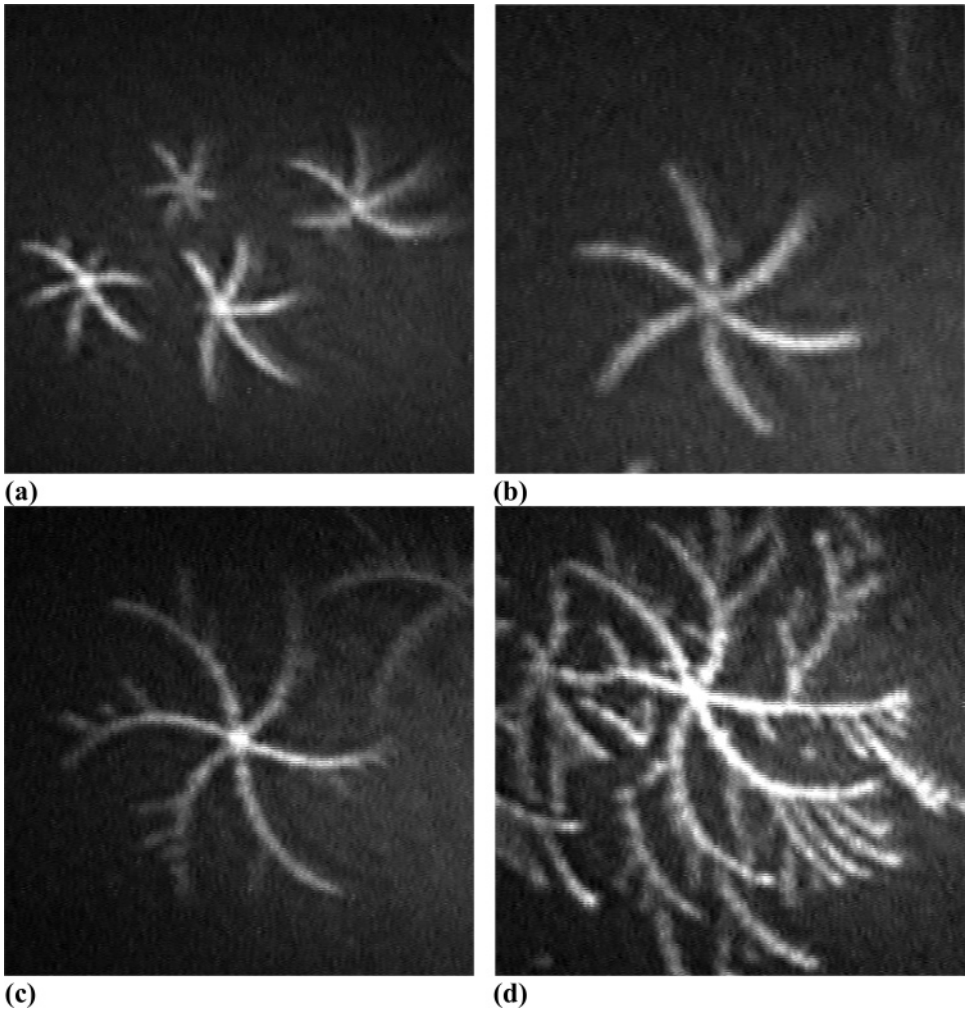

Figure 7. Succeeding stages of the domain development within the phase coexistence region of the $\pi-A$ isotherms of THPA monolayer spread on water, obtained for higher compression rates (>0.1 nm^2/(min molecule)); $T = 10$ °C. Domain arms and axes are curved in one direction.

to demonstrate in which way the exchange in the position of the two substituents at the acid amide group affects the morphology of the condensed phase domains.

At first, the formation and growth of the condensed phase domains of the HETA monolayer within the phase coexistence region at 20 °C are illustrated (Figure 5). After the phase transition point π_c at the beginning of the plateau region, first small domains of compact and nearly round shape are formed (Figure 5a). At slow compression of the monolayer, rather thick arms (in most cases, six) grow from the compact center in all directions (Figure 5b). Already, in the initial state they are irregularly shaped. Striking features of the domain shape are not only the differences in the averaged thickness of the main axes but also a different thickness growth of the single bent arms with conspicuous thickening at the tip. The fractal nature of the domain shape and the absence of an inner texture of the domains becomes obvious in the further stages of the domain growth (Figure 5c,d). These characteristics indicate a certain fluidity of the condensed phase. The domain growth is obviously based on tip splitting under the formation of numerous doubloons, and thus branching is considerably limited. It is interesting to note that the bright HETA domains are homogeneously reflecting. This suggests an orientation of the alkyl chains perpendicular to the aqueous surface.

The features of the THPA condensed phase domains are completely different (demonstrated for $T = 10$ °C in Figures 6−8). It is obvious that the main difference results from the higher crystallinity of the THPA condensed phase in comparison to that of HETA. Also, in the case of THPA monolayers, the formation of the condensed phase domains starts after the main phase transition point at the beginning of the plateau region of the $\pi-A$ isotherms at all temperatures (see Figure 3). At the beginning, six straight main axes grow from a round center in a regular distance of about 60 degrees from each other (Figure 6a). The bright condensed phase domains are surrounded by the fluid phase of lower density and thus lower reflectivity. In the succeeding stages of growth, the main axes develop numerous straight branches on both sides, clearly indicating the dendritic character of the domain shape (Figure 6b−d). In agreement with experimental results of other amphiphiles containing an acid amide group, the stability of the dendritic domains is remarkably high so that a rearrangement to a compact equilibrium shape could not be observed.

At higher compression rates (>0.1 nm^2/(min molecule)), the domain shape changes. Although the general features are preserved, the main axes and side branches are curved under these conditions. Higher compression rates facilitate the formation of dislocations in the 2D lattice structure as a precondition for the development of curved dendrites. The changes in the orientation of such curvatures are caused by dislocations along a small angle grain line. Figure 7 shows different steps of the domain growth with all arms curved in one direction (counterclockwise in the present case). However, in numerous domains, a curvature of the arms in opposite directions (clockwise and

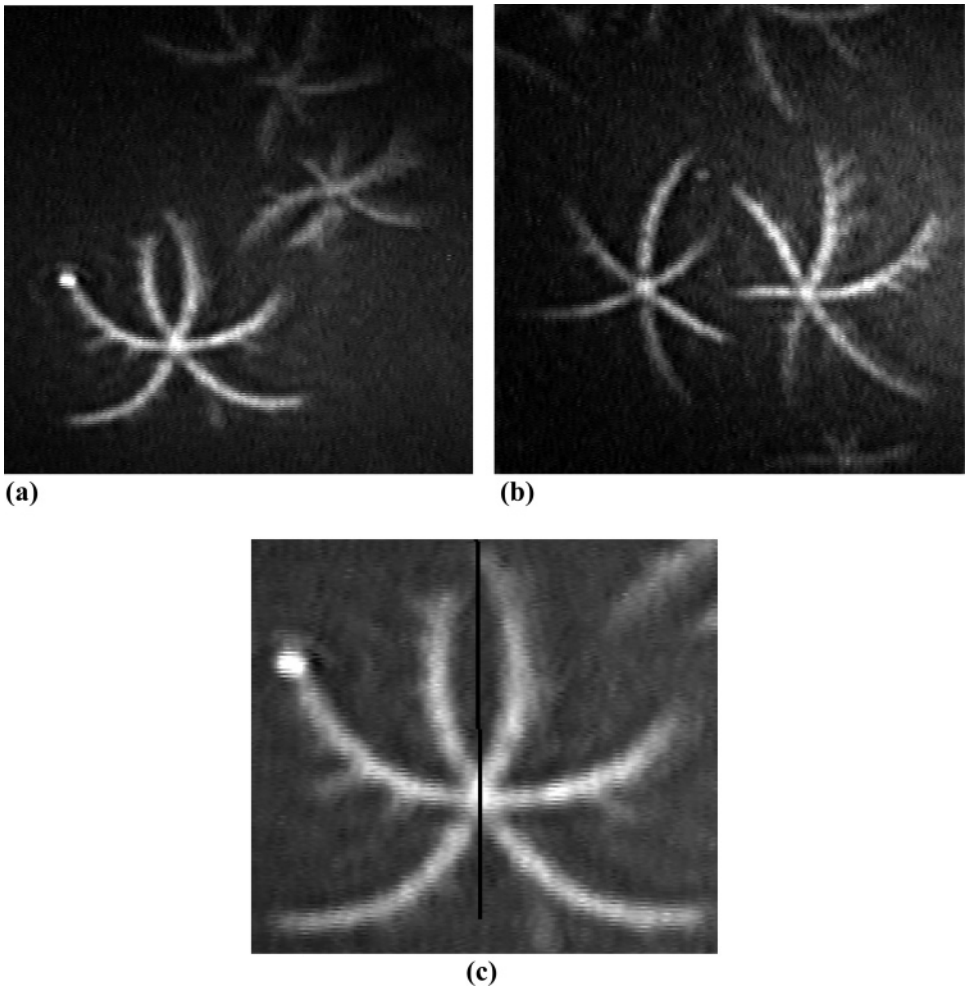

Figure 8. Domains, having axes and arms curved in opposite direction, formed within the phase coexistence region of the $\pi-A$ isotherms of a THPA monolayer spread on water, obtained for higher compression rates (>0.1 nm^2/(min molecule)). Three dendrite arms are curved clockwise, and the other three arms are curved counterclockwise. Such domains represent 2D twins. $T = 10$ °C.

counterclockwise) can be observed (left domain in Figure 8a,b). It is interesting to note that three dendrite arms are always curved clockwise, and the other three arms are curved counterclockwise. In all these cases, the domain shape is subdivided into two halves that have a mirror-image relation. This is demonstrated by the black line in Figure 8c. These domain types can be considered to be 2D twins. Twinning is a lattice defect that occurs in three-dimensional crystals.[36] Different partial lattices can be transformed into each other by the addition of a symmetry element such as a mirror plane or an axis. This concept has been analogously introduced for 2D monolayers when subdomains are separated by mirror lines.[37,38]

GIXD studies provide additional information about the structure of the condensed monolayer phases. Therefore, these studies should clarify the extent to which the exchange in the position of the two substituents at the acid amide group affects the lattice structure of the monolayers. In the case of HETA monolayers, only one diffraction peak has been observed. Figure 9 shows two selected contour plots of the corrected intensities as a function of the in-plane scattering vector component Q_{xy} and the out-of-plane scattering vector component Q_z for HETA monolayers at $\pi = 20$ mN/m obtained for different temperatures (10 and 20 °C). In all cases studied, only one diffraction peak was observed, indicating a hexagonal packing of the HETA molecules oriented perpendicularly to the surface in an LS phase. For some HETA monolayers measured at different conditions, the Bragg peak positions, their full widths at half-maximum (ΔQ_{xy}), and the lattice parameters are listed in Table 1. As seen from Table 1, the monolayers were stable enough to be compressed to ≥20 mN/m at 10 and 20 °C, respectively. Particularly, the data obtained at $T = 20$ °C show that the position of the Bragg peak shifts to larger Q_{xy} values as the surface pressure increases. Therefore, the area of the unit cell, A_{xy} decreases slightly from 0.204 nm^2 at 6 mN/m to 0.202 nm^2 at 22 mN/m. At the same surface pressures, the Q_{xy} values are larger at lower temperatures, and thus, as expected, the A_{xy} values are lower ($A_{xy} = 0.199$ nm^2 at $T = 10$ °C, $A_{xy} = 0.202$ nm^2 at $T = 20$ °C). These values of the cross-sectional area indicate a certain mobility of the molecules that are in a rotator phase. The coherence lengths, ξ, were calculated on the basis of the measured ΔQ_{xy} values corrected by the horizontal resolution, mainly given by the Soller collimator.[39] This gives rise to ξ values of 550 Å ≤ ξ ≤600 Å for the lower temperature (10 °C). It is interesting to note that, at the higher temperature (20 °C), the full widths at half-maximum of the in-plane diffraction peak are below or at the resolution limit of $\Delta Q_{xy} \approx 0.008$ Å^{-1} up to a comparably high surface pressure of 20 mN/m. This suggests a more homogeneous growth of the LS phase under these conditions. In all measured examples, the Bragg rods have a medium full width at half-maximum, $\Delta Q_z \approx 0.347$ Å^{-1}. If a flat oblate ellipsoid is used for the all-trans conformation of the alkyl chain,[13] then the measured ΔQ_z value is related to the alkyl chain length, L, by $\Delta Q_z = 2\pi/L$. The value of $L =$ 18.1 Å calculated for the scatterer agrees reasonably well with

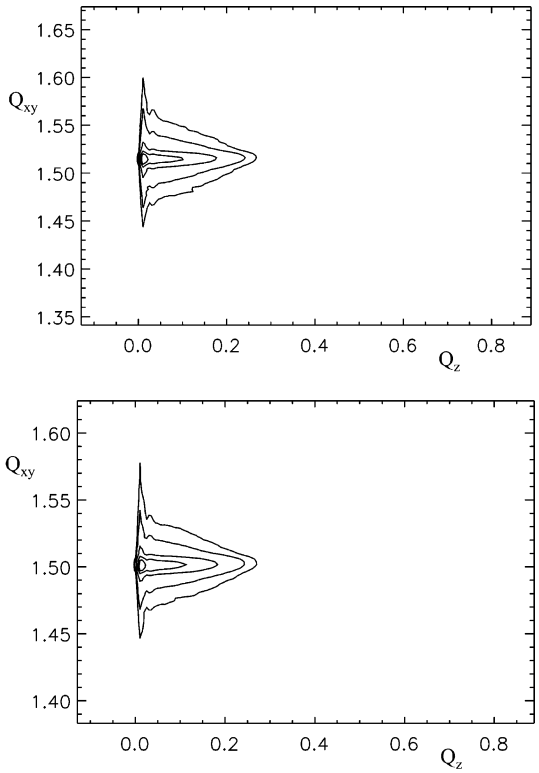

Figure 9. GIXD contour plots of the corrected diffraction intensities as a function of the in-plane (Q_{xy}) and out-of-plane (Q_z) components of the scattering vectors for HETA monolayers at 20 mN/m: (top) $T = 10$ °C and (bottom) $T = 20$ °C.

TABLE 1: GIXD Results of HETA Monolayers

T (°C)	π (mN/m)	peak position Q_{xy} (Å^{-1})	full width at half maximum ΔQ_{xy} (Å^{-1})	cell parameters $a = b = c$ (Å)	unit cell area $A_{xy} = A_0$ (Å^2)	coherence length ξ (Å)
10	15	1.51318	0.01377	4.79	19.9	560
10	20	1.51491	0.01341	4.79	19.9	583
20	6	1.49398	0.00715	4.86	20.4	
20	20	1.50091	0.00810	4.83	20.2	
20	22	1.50151	0.01096	4.83	20.2	838

the extended $C_{13}H_{27}$ alkyl chain under consideration of the van der Waals radii ($L = 18.3$ Å).

The lattice structure of the TMPA monolayers is completely different. It was of special interest to obtain more information about the existence of two different condensed phases because of the second phase transition between two condensed phases, as observed in the $\pi-A$ isotherms at low temperatures (<10 °C; see Figure 9). Figure 10 shows two representative contour plots of the corrected intensities as a function of the in-plane scattering vector component Q_{xy} and the out-of-plane scattering vector component Q_z for TMPA monolayers obtained at 2 °C in the main phase coexistence region at $\pi = 12$ mN/m, and above the second phase transition between the two condensed phases at $\pi = 24$ mN/m. Table 2 gives the peak positions of the in-plane and the out-of-plane scattering vectors (Q_{xy}, Q_z) at several surface pressures studied. Three scattering peaks generally indicate an oblique lattice for both condensed phases. However, it is clearly seen that the positions of the Bragg peaks, and thus also their scattering vector components, change drastically at the surface pressure, indicating a second transition between two condensed phases. This results in an abrupt change of the 2D lattice structure at the transition surface pressure at low temperatures (see Table 3). On the other hand, the lattice

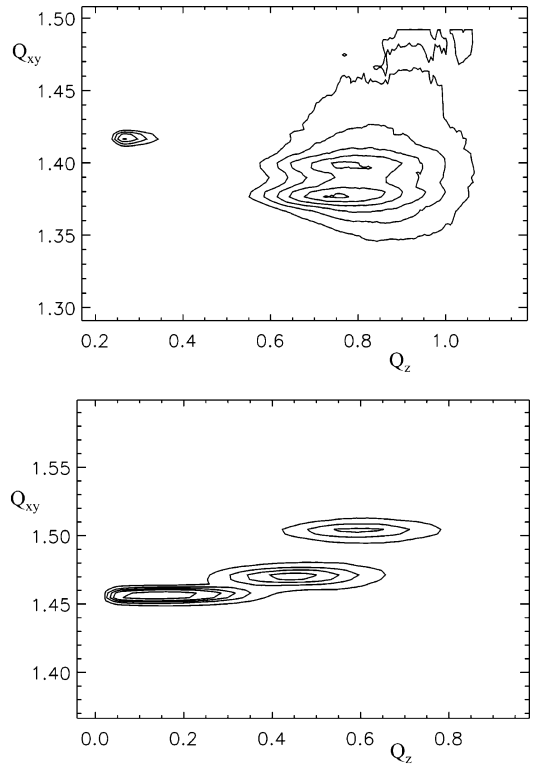

Figure 10. GIXD contour plots of the corrected diffraction intensities as a function of the in-plane (Q_{xy}) and out-of-plane (Q_z) components of the scattering vectors for THPA monolayers at 2 °C: (top) $\pi = 12$ mN/m and (bottom) $\pi = 24$ mN/m.

TABLE 2: Scattering Vector Components of the Three Reflections (In-Plane (Q_{xy}) and Out-of-Plane (Q_z) Components) of THPA Monolayers[a]

π (mN/m)	(10) Q_{xy} (Å^{-1})	(10) Q_z (Å^{-1})	(01) Q_{xy} (Å^{-1})	(01) Q_z (Å^{-1})	(11) Q_{xy} (Å^{-1})	(11) Q_z (Å^{-1})
12	1.37721	0.27525	1.3976	0.81483	1.41535	0.79906
18	1.40112	0.28388	1.42566	0.72164	1.45516	0.75552
20	1.45973	0.58593	1.46487	0.07502	1.50001	0.44629
24	1.45663	0.60619	1.47073	0.46115	1.50353	0.16389
30	1.45717	0.59179	1.47832	0.43715	1.50975	0.16353

[a] $T = 2$ °C.

TABLE 3: Lattice Parameters of PMTA Monolayers[a]

π (mN/m)	a (Å)	b (Å)	c (Å)	γ (deg)	t (deg)	A_{xy} (Å^2)	A_0 (Å^2)	ψ_a (deg)	d
12	5.12	5.20	5.27	118.7	34.0	23.4	19.5	19.8	0.0315
18	4.99	5.08	5.19	118.0	31.2	22.4	19.3		0.0438
20	4.87	4.89	5.01	118.3	25.0	21.0	19.2	65.8	0.0345
24	4.83	4.90	4.99	118.4	25.3	20.8	19.1	74.5	0.0367
30	4.82	4.89	4.99	118.1	24.8	20.8	19.1	74.6	0.0413

[a] $T = 2$ °C. π is surface pressure; a, b, c, and γ are lattice constants; t is polar tilt angle; A_{xy} is molecular area; A_0 is the cross-section area of alkyl chain; ψ_a is the angle between the azimuthal tilt direction and the a-axis; and d is distortion.

constants a, b, c, and γ, the polar tilt angle τ, and the unit cell area A_{xy} decrease only weakly both below the phase transition pressure and above it. The surface pressure dependence of the unit cell (cross-sectional) area A_{xy} is demonstrated in Figure 11, and that of the polar tilt angle τ in shown in Figure 12. It is seen that, in the surface pressure range between the two phase transitions shown in Figure 3 (1−16 mN/m), both A_{xy} and τ decrease linearly with the increase in the surface pressure. Above the second phase transition (20 mN/m and higher), A_{xy} as well as τ of the THPA monolayer decrease only slightly in the higher

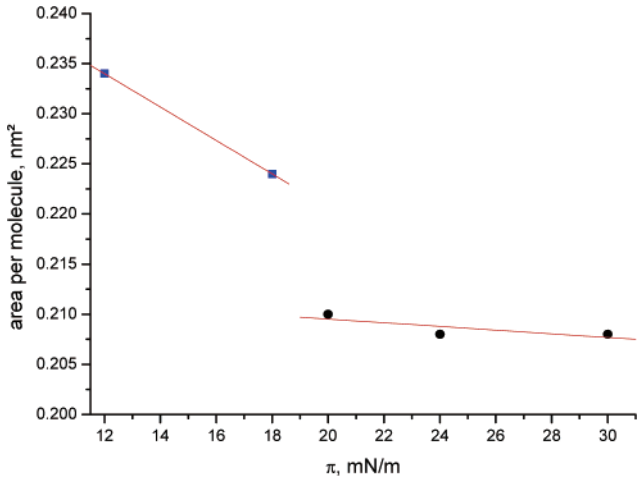

Figure 11. Dependence of the unit cell (cross-section) area A_{xy} of a THPA monolayer on surface pressure π, obtained by GIXD. See detailed discussion in the text.

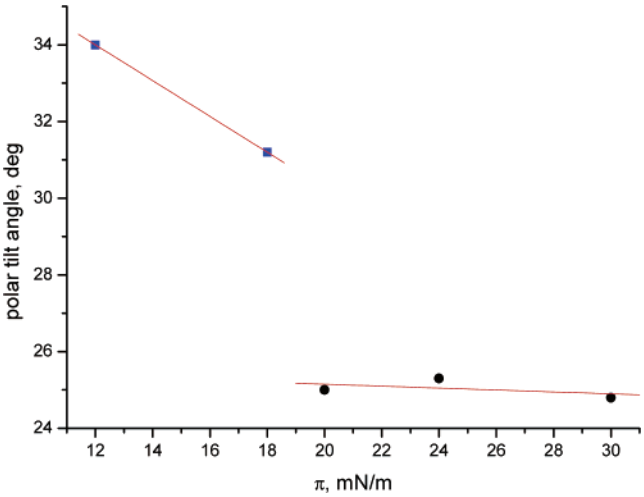

Figure 12. Dependence of the polar tilt angle of the THPA monolayer molecules on surface pressure π, obtained by GIXD. See detailed discussion in the text.

surface pressure range, so that here the slope obtained by linear fitting is essentially lower than it is in the region of the first condensed phase. However, at a surface pressure value between 18 and 20 mN/m, which approximately corresponds to the second inflection point of the $\pi-A$ isotherm in Figure 3, the area per THPA molecule in the condensed state changes drastically. The second phase transition between the two condensed phases is obviously characterized by an abrupt change in the lattice structure. The linear variation of the polar tilt angle τ and the unit cell area A_{xy} within the range, where a definite condensed phase exists, is correlated with the 2D compressibility of condensed monolayer phases.[40]

Conclusion

The synthesis of the tailored amphiphiles THPA and HETA allows the comparison of the monolayer characteristics of two very similar amphiphiles, the chemical structure of which is only changed by exchanging the position of the two substituents at the acid amide group. These small changes in the chemical structure give rise to large differences in the monolayer features, as demonstrated by coupling the $\pi-A$ isotherms, BAM imaging, and GIXD measurements.

The linear relationship between the fluid/condensed phase transition pressure π_c and the temperature shows large differences in the phase behavior of the HETA and THPA monolayers. Since both amphiphiles have the same alkyl chain length, the π_c-T shift from THPA to HETA at higher temperatures indicates the stronger polar character of the THPA headgroup. The features of the $\pi-A$ isotherms of HETA, having a sharp inflection at the first-order phase transition point (A_c) from the fluid phase to the condensed phase, correspond to those of most of the usual monolayers of amphiphiles. The $\pi-A$ isotherms of the THPA monolayers reveal an additional cusp at $T < 10$ °C, which suggests a further phase transition between two condensed phases.

Considerable differences between the HETA and THPA monolayers exist also in the domain morphology, although, in both cases, six arms usually grow from a round center. The characteristic shapes of the HETA domains are developed by tip splitting under the formation of numerous doubloons so that branching is considerably limited. The fractal shape suggests a certain fluidity of the HETA condensed phase. The main differences of the THPA domains result from the higher crystallinity. Starlike domains of dendritic character are formed.

Higher compression rates facilitate the development of curved dendrites, which are partially 2D twins due to the formation of dislocations in the 2D lattice structure.

GIXD studies of the two amphiphiles reveal large differences in the 2D lattice structure of their monolayers. In the case of HETA monolayers, a hexagonal packing of the alkyl chains oriented perpendicularly to the surface in an LS phase exists in the accessible temperature range. The high values of the cross-sectional area indicate a certain mobility of the molecules that are in a rotator phase. In the case of THPA monolayers, three scattering peaks generally indicate an oblique lattice structure for both condensed phases. However, at the surface pressure, indicating a second transition between two condensed phases at low temperatures, the main characteristics of the lattice data change abruptly. This can be convincingly demonstrated by the surface pressure dependence of the polar tilt angle of the molecules and the cross-section area per molecule. Thus, the second phase transition between the two condensed phases is due to an abrupt transition between two different oblique lattice structures.

References and Notes

(1) McConnell, H. M.; Moy, V. T. *J. Phys. Chem.* **1988**, *92*, 4520.
(2) Vanderlick, T. K.; Möhwald, H. *J. Phys. Chem.* **1990**, *94*, 886.
(3) Deutch, J. M.; Low, F. E. *J. Phys. Chem.* **1992**, *96*, 7097.
(4) Miranda, J. A. *J. Phys. Chem. B* **1999**, *103*, 1303.
(5) Vollhardt, D. *Adv. Colloid Interface Sci.* **1996**, *64*, 143.
(6) Vollhardt, D. In *Encyclopedia of Surface and Colloid Science*; Hubbard, A., Ed.; Marcel Dekker: New York, 2002; p 3585.
(7) Vollhardt, D. *Adv. Colloid Interface Sci.* **1999**, *79*, 19.
(8) Vollhardt, D.; Fainerman, V. B. *Adv. Colloid Interface Sci.* **2000**, *86*, 103−151.
(9) Fainerman, V. B.; Vollhardt, D. In *Organized Monolayers and Assemblies: Structure, Processes and Function*; Möbius, D., Miller, R., Eds.; Elsevier: Amsterdam, 2002; Vol. 16, pp 105−160.
(10) Vollhardt, D.; Liu, F.; Rudert, R. *ChemPhysChem* **2005**, *6*, 1246.
(11) Vollhardt, D.; Liu, F.; Rudert, R.; He, W. *J. Phys. Chem. B* **2005**, *109*, 10849.
(12) Vollhardt, D.; Fainerman, V. B.; Liu, F. *J. Phys. Chem. B* **2005**, *109*, 11706.
(13) Thirumoorthy, K.; Nandi, N.; Vollhardt, D. *J. Phys. Chem. B* **2005**, *109*, 10820.
(14) Weidemann, G.; Vollhardt, D. *Biophys. J.* **1996**, *70*, 2758.
(15) Vollhardt, D.; Siegel, S.; Cadenhead, D. A. *Langmuir* **2004**, *20*, 7670. *J. Phys. Chem. B* **2004**, *108*, 17448.
(16) Berg, J. M.; Tymoczko, J. L.; Stryer, L. *Biochemistry*, 5th ed.; W. H. Freeman & Co.: New York, 2003; p 324.
(17) Nelson, D. L.; Cox, M. M. *Lehninger, Principles of Biochemistry*, 4th ed.; W. H. Freeman & Co.: New York, 2004; p 353.
(18) Hühnerfuss, H.; Neumann, V.; Stine, K. J. *Langmuir* **1996**, *12*, 256.

(19) Mobelli, E.; Morris, R.; Taylor, W.; Fraternali, F. *Biophys. J.* **2003**, *84*, 1507.
(20) Melzer, V.; Vollhardt, D. *Phys. Rev. Lett.* **1996**, *76*, 3770.
(21) Vollhardt, D.; Melzer, V. *J. Phys. Chem. B* **1997**, *101*, 3370.
(22) Melzer, V.; Weidemann, G.; Vollhardt, D.; Brezesinski, G.; Wagner, R.; Struth, B.; Möhwald, H. *J. Phys. Chem. B* **1997**, *101*, 4752.
(23) Melzer, V.; Weidemann, G.; Vollhardt, D.; Brezesinski, G.; Wagner, R.; Struth, B.; Möhwald, H. *Supramol. Sci.* **1997**, *4*, 391.
(24) Melzer, V.; Vollhardt, D. *Prog. Colloid Polym. Sci.* **1997**, *105*, 1130.
(25) Melzer, V.; Vollhardt, D.; Brezesinski, G.; Möhwald, H. *J. Phys. Chem B* **1998**, *102*, 591.
(26) Melzer, V.; Vollhardt, D.; Weidemann, G.; Brezesinski, G.; Wagner, R.; Möhwald, H. *Phys. Rev. E* **1998**, *57*, 901.
(27) Vollhardt, D.; Melzer, V.; Fainermann, V. B. *Thin Solid Films* **1998**, *327*−*329*, 842.
(28) Melzer, V.; Vollhardt, D.; Brezesinski, G.; Möhwald, H. *Thin Solid Films* **1998**, *327*−*329*, 857.
(29) Melzer, V.; Weidemann, G.; Wagner, R.; Vollhardt, D.; DeWolf, C.; Brezesinski, G.; Möhwald, H. *Chem. Eng. Technol*. **1998**, *21*, 44.
(30) Fainerman, V. B.; Vollhardt, D. *J. Phys. Chem. B* **2003**, *107*, 3098.
(31) Meunier, J. *Colloids Surf. A* **2000**, *171*, 33.
(32) Kaganer, V. M.; Möhwald, H.; Dutta, P. *Rev. Mod. Phys*. **1999**, *71*, 779.
(33) Als-Nielsen, J.; Möhwald, H. In *Handbook on Synchrotron Radiation*; Ebashi, S., Koch, M., Rubenstein, E., Eds.; Elsevier: Amsterdam; Oxford; New York; Tokyo, 1994; Vol. 4, pp 1−53.
(34) Als-Nielsen, J.; Kjaer, K. In *Phase Transitions in Soft Condensed Matter*; Riste, T., Sherrington, D., Eds.; NATO ASI Series B; Plenum Press: New York, 1989; Vol. 211, p 113.
(35) Fainerman, V. B.; Vollhardt, D. *J. Phys. Chem. B* **1999**, *103*, 145.
(36) Kleber, W. *An Introduction to Crystallography*; VEB Verlag Technik: Berlin, 1970.
(37) Moy, V. T.; Keller, D. J.; Gaub, H. E.; McConnell, H. M. *J. Phys. Chem.* **1986**, *90*, 3198.
(38) McConnell, H. M. *Annu. Rev. Phys. Chem.* **1991**, *42*, 171.
(39) Kjaer, K. *Physica B* **1994**, *198*, 100.
(40) Kaganer, V. M.; Brezesinski, G.; Möhwald, H. *Phys. Rev. E* **1999**, *59*, 2141.